Review



# Electrochemical Aptamer-Based Sensors for In Vivo Pharmacokinetic Monitoring of Anthracycline Chemotherapeutics: Mechanisms, Stability, and the Clinical Translation Landscape

Haoran Zhang , Huixin Wang , Wen Luo * , Tao Liu *

Posted Date: 2 June 2026

doi: 10.20944/preprints202606.0143.v1

Keywords: electrochemical aptamer-based sensor; anthracycline; doxorubicin; daunorubicin; therapeutic drug monitoring; pharmacokinetics; FFT-EIS; xenonucleic acid; antifouling; clinical translation

 doi:10.20944/preprints202606.0143.v1



*Review*

# Electrochemical Aptamer-Based Sensors for In Vivo Pharmacokinetic Monitoring of Anthracycline Chemotherapeutics: Mechanisms, Stability, and the Clinical Translation Landscape

**Haoran Zhang [1], Huixin Wang [2], Wen Luo [3,*] and Tao Liu [4,*]**

[1] School of Pharmacy, Guangdong Pharmaceutical University, Guangzhou 510006, China
[2] The First Clinical Medical College, Guangdong Pharmaceutical University, Guangzhou 510006, China
[3] Key Laboratory of Renewable Energy, Guangdong Key Laboratory of New and Renewable Energy Research and Development, Guangzhou Institute of Energy Conversion, Chinese Academy of Sciences, Guangzhou 510640, China
[4] School of Basic Medical Sciences, Guangdong Pharmaceutical University, Guangzhou 510006, China
* Correspondence: luowen@ms.giec.ac.cn (W.L.); liutao@gdpu.edu.cn (T.L.)

**Abstract**

Anthracycline agents, principally doxorubicin and daunorubicin, are widely used in oncology yet carry a narrow therapeutic index and pronounced interindividual pharmacokinetic variability that exposes patients simultaneously to the risk of subtherapeutic dosing and cumulative cardiotoxicity. Conventional therapeutic drug monitoring (TDM) based on periodic venous sampling and offline high-performance liquid chromatography cannot resolve the sub-minute concentration dynamics that determine organ-specific drug exposure. Electrochemical aptamer-based (EAB) sensors couple nucleic-acid aptamers, self-assembled monolayers, and methylene blue redox reporters on gold microelectrodes to convert binding-induced conformational changes into real-time, reagent-free electrochemical signals. Recent advances in this field fall into five areas: signal interrogation strategies, from kinetic differential measurement to calibration-free Fourier-transform impedance spectroscopy (FFT-EIS); interface engineering including nanostructured electrodes and AI-guided aptamer design; in vivo multi-compartment pharmacokinetic monitoring and closed-loop feedback drug delivery; the mechanisms of in vivo signal drift alongside antifouling countermeasures spanning hydrogel barriers, zwitterionic brushes, and xenonucleic acid backbone substitution; and FDA premarket pathways and clinical translation, including Premarket Approval requirements and the emerging Real-Time Clinical Trial (RTCT) framework. In live rodents, dual-compartment monitoring has resolved a reproducible 30–60 minutes plasma-to-ISF lag for doxorubicin at 12-second temporal resolution; calibration-free FFT-EIS interrogation achieves inter-animal coefficients of variation below 12% without individual pre-calibration; and xenonucleic acid backbone substitution has extended continuous in vivo operation to seven consecutive days. Three gaps still separate rodent proof-of-concept work from chemotherapy patients: clinical-context validation, tumor microenvironment calibration, and anthracycline-specific XNA aptamer design.

**Keywords:** electrochemical aptamer-based sensor; anthracycline; doxorubicin; daunorubicin; therapeutic drug monitoring; pharmacokinetics; FFT-EIS; xenonucleic acid; antifouling; clinical translation

## 1. Introduction

*1.1. Clinical Significance of Anthracyclines and the Need for TDM*

 doi:10.20944/preprints202606.0143.v1



Anthracyclines, including doxorubicin and daunorubicin, remain standard agents in contemporary combination chemotherapy for acute leukemias, breast cancer, sarcomas, and lymphomas [1], exerting cytotoxicity primarily through topoisomerase II inhibition and DNA intercalation [2]. Despite decades of clinical experience, dosing remains predominantly weight- or body-surface-area (BSA)-based, a convention that correlates poorly with individual area under the curve (AUC) values [3,4]. Multiple prospective studies have documented substantial (often exceeding fivefold) interpatient variability in plasma exposure at identical nominal doses, driven by polymorphisms in carbonyl reductases (e.g., CBR1/3) and drug efflux transporters [5,6]. Underdosed patients face compromised tumor response; overdosed patients accumulate cardiac exposure that may precipitate irreversible anthracycline-induced cardiomyopathy, whose incidence rises sharply beyond 400 mg/m$^2$ of doxorubicin equivalent [7,8].

An underappreciated contributor to pharmacokinetic heterogeneity is the gut microbiome. Certain intestinal bacteria, notably *Raoultella planticola*, harbor molybdopterin-dependent oxidoreductases capable of reductive deglycosylation of doxorubicin under anaerobic conditions, converting it to less active aglycone metabolites whose production varies widely across individuals depending on diet, prior antibiotic exposure, and microbiota composition [9]. Real-time, patient-specific drug-level data would capture the net pharmacokinetic outcome of this multifactorial variability, making continuous TDM more informative than genotype-only or BSA-based predictions alone [4].

### *1.2. Limitations of Conventional Monitoring Approaches*

Serial venipuncture followed by reversed-phase HPLC or LC-MS/MS remains the clinical gold standard for anthracycline quantification, providing confirmed specificity and nanomolar-range sensitivity [10,11]. The principal limitation is temporal: even intensive sampling protocols, typically four to eight time points over six hours, cannot capture the rapid distribution phase during which plasma concentrations fall by an order of magnitude within the first thirty minutes after bolus infusion [3,12]. As shown in Figure 1A,B, a continuous kinetic lag separates plasma and the interstitial compartment—dynamics that discrete sampling generally misses. Peak cardiac exposure, rather than cumulative AUC alone, has been linked to acute myocardial injury in preclinical models [13]. Implantable microdialysis probes can access interstitial fluid (ISF) in real time but introduce their own distortions: continuous perfusion dilutes local bioactive concentrations, probe insertion elicits inflammatory tissue responses that alter local drug transport [14], and the extraction efficiency of amphiphilic small molecules such as anthracyclines is severely hindered by non-specific hardware adsorption and slow transmembrane transport kinetics [15–17].

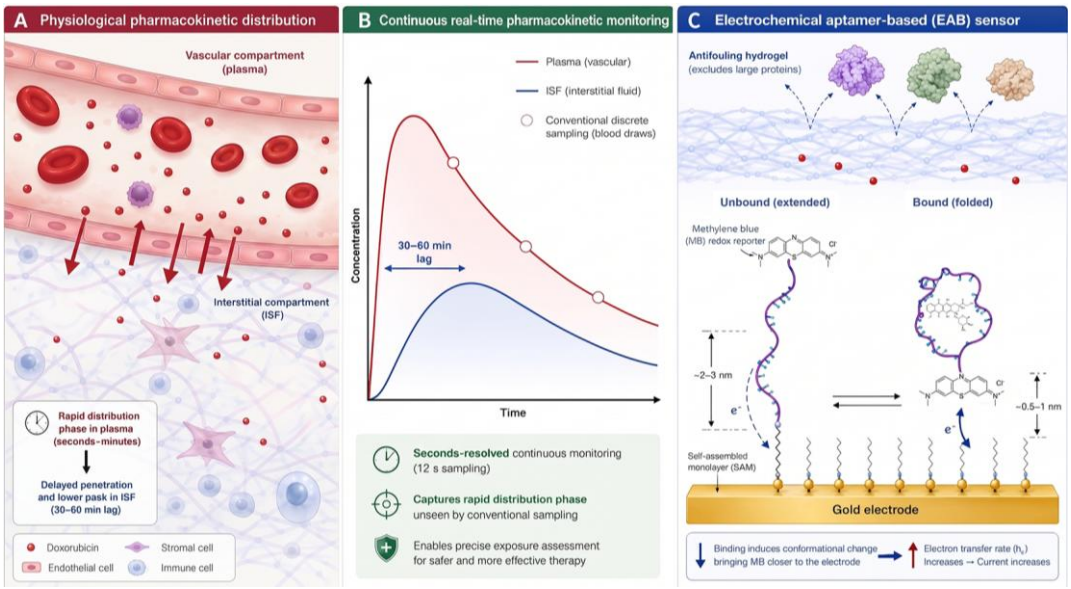

 doi:10.20944/preprints202606.0143.v1



**Figure 1.** Pharmacokinetic distribution and EAB sensor mechanisms. (A) Drug transport from the vascular compartment (plasma) to the interstitial fluid (ISF), illustrating the delayed penetration phase. (B) Continuous monitoring profiles showing the pharmacokinetic lag between plasma and ISF compared to conventional discrete sampling methods. (C) Sensor interface on a gold electrode. An outer antifouling hydrogel excludes large proteins. The inner self-assembled monolayer contains aptamers that undergo a binding-induced conformational change, reducing the distance between the methylene blue (MB) reporter and the electrode to alter the electron transfer rate.

### *1.3. EAB Sensors: Operating Principle and Distinct Advantages*

Electrochemical aptamer-based (EAB) sensors address these limitations through a reagentless, reversible operating principle. A thiolated nucleic-acid aptamer modified with a methylene blue (MB) redox reporter at its distal terminus is immobilized on a gold microelectrode within a self-assembled monolayer (SAM) of passivating alkanethiols [18,19]. Ligand binding induces a conformational change, typically a coil-to-fold transition that alters the distance and electronic coupling between MB and the gold surface. As shown in Figure 1C, this modifies the apparent heterogeneous electron-transfer rate constant, $k_0$ [20]. This rate shift is transduced into a quantitative current signal by electrochemical interrogation methods that selectively probe faradaic processes [21]. Neither the aptamer nor the electrode material participates catalytically, so the sensor operates in complex, undiluted biological matrices without added reagents. Early demonstrations in awake rodents used square-wave voltammetry (SWV) to track cocaine and tobramycin at ten-second resolution [22]; subsequent work extended the platform to doxorubicin and daunorubicin as clinically relevant anthracycline targets [23–25]. Sections 2–5 cover interface engineering, in vivo pharmacokinetics, stability, and regulatory translation.

## 2. Signal Transduction Mechanisms and Interface Engineering

### *2.1. Aptamer Design: Truncation, Surface Density, and AI-Assisted Engineering*

Small-molecule-binding aptamers identified by SELEX frequently require structural optimization before they can function effectively as EAB sensor components [26,27]. A truncated aptamer must simultaneously retain sufficient affinity to cover the clinical concentration window—typically 0.1–5 μM for doxorubicin following standard infusion doses [28], and preserve enough conformational flexibility to produce measurable signal gain upon binding [29]. Shaver et al. illustrated that these objectives can conflict: a single base-pair truncation in the stem of the vancomycin aptamer that reduced stem-loop stability improved the in vivo signal-to-noise ratio (SNR) from 1.03 to 1.62, shifting the dynamic range into the pharmacologically relevant window; however, excessive truncation collapsed the affinity from Kd ~ 3.9 μM to 45 μM, rendering the sensor unusable during trough periods [30]. Nguyen et al. extended this principle by demonstrating that in silico docking of truncated aptamer variants against target small molecules correlates with experimental signal gain, offering a computational alternative to empirical truncation screens [31].

Surface probe density introduces an orthogonal variable. White et al. established that sub-saturating probe packing, achieved by diluting the aptamer thiol with a spacer alkanethiol, can improve signal gain by relieving steric constraints on conformational switching, though the minimum density maintaining adequate current amplitude must be empirically determined for each aptamer-target pair [32]. Freeze-thaw directed assembly has since been proposed to reduce inter-electrode variability in SAM formation by aligning thiolated DNA molecules in an extended conformation before annealing [33].

Diffusion-model-based aptamer design has advanced rapidly. Wang et al. introduced AptaDiff, a discrete diffusion model guided by Bayesian optimization, which generated dissociation constants two- to fourfold lower than SELEX candidates for protein targets initially tested [34]. Baek et al. concurrently reported RoseTTAFoldNA, extending RoseTTAFold to model nucleic acid tertiary structures in protein–nucleic acid complexes with predicted template modeling (pTM) scores

 doi:10.20944/preprints202606.0143.v1



validated against solved crystal structures [35]. Neither tool has yet been applied to anthracycline-specific aptamer engineering in published reports or validated experimentally for doxorubicin or daunorubicin aptamers; moreover, RoseTTAFoldNA remains optimized for large protein–nucleic acid complexes, and its capacity to predict small-molecule docking geometry within dynamic aptamer binding pockets is still unproven. Table 1 also lists MAWS and AptaLoop as iGEM competition software repositories.

**Table 1.** Computational tools for aptamer design relevant to EAB sensor engineering.

| Computational Tool | Algorithmic Mechanism | Target Application and Validation Status | Key Limitations | Ref |
|---|---|---|---|---|
| **AptaDiff** | Generative discrete diffusion model with Bayesian optimization for affinity-guided sequence generation in a motif-dependent latent space | De novo sequence generation; $K_d$ reductions 2–4× vs SELEX candidates for protein targets; anthracycline validation pending | Validated mainly for protein targets; small-molecule benchmarks remain limited | [34] |
| **MAWS** | Entropy-minimization algorithm driving progressive nucleotide selection based on Kullback-Leibler divergence | IGEM open-source repository; eliminates requirement for initial physical oligonucleotide pool; useful for rational small-molecule aptamer design | Structural accuracy depends heavily on force-field calibration quality (e.g., AMBER parameters) | [36] |
| **AptaLoop** | Computational pipeline integrating secondary structure prediction, MAWS, AutoDock Vina, and molecular dynamics | IGEM open-source pipeline for general aptamer-ligand evaluation; applied to environmental (e.g., PFAS) biosensor development | Does not natively account for EAB electrochemical interface effects or explicitly predict signal transduction | [37] |
| **In Silico Docking & Truncation** | Structural docking of iteratively truncated aptamer sequences to map essential functional binding domains | Correlates drug-aptamer docking parameters with experimental EAB signal gain to optimize truncation length | Truncation space requires empirical validation of redox reporter collision dynamics and SAM sterics | [31] |
| **RoseTTAFoldNA** | RoseTTAFold 3-track neural network framework extended to protein–nucleic acid complexes; generates 3D models with confidence scores | High-confidence structural prediction for aptamer-target complexes; enables rational binding-site engineering | Primarily validated for large complexes; small-molecule binding geometry and dynamics less well characterized | [35] |

Ref: cited reference; MAWS, Making Aptamers Without SELEX; SELEX, systematic evolution of ligands by exponential enrichment; PFAS, per- and polyfluoroalkyl substances.

### *2.2. Nanostructured Electrodes and Signal Amplification*

The absolute faradaic current from a planar gold microelectrode (diameter ≈ 200 μm) limits achievable detection sensitivity, which nanostructured interfaces address through increased roughness and available surface area [38]. Jahani et al. modified screen-printed carbon electrodes with NiO nanosheets, achieving a nanomolar detection limit (~3 nM) for daunorubicin by differential pulse voltammetry [39]. In vivo studies have used nanoporous gold EAB systems: Qin et al. demonstrated hours-long continuous daunorubicin tracking in rat blood, resolving pharmacokinetic

 doi:10.20944/preprints202606.0143.v1



parameters including distribution and elimination half-lives directly from the sensor output [23]. Nanoconfined aptamer constructs, in which aptamer strands are tethered inside nanoscale cavities that concentrate target analytes while restricting nonspecific interactions, offer one route to higher sensitivity and reduced biofouling [40].

Flexible electrodes are being developed in parallel. Laser-induced graphene and MOF-derived porous carbons patterned on polyimide substrates yield electrodes that conform to tissue surfaces without mechanical damage [41,42]. For long-term monitoring in vascularly constrained or subcutaneous anatomical locations, mechanical compliance can reduce the foreign-body response that accelerates biofouling and signal loss [43].

### *2.3. Signal Interrogation: From SWV to Calibration-Free FFT-EIS*

The performance ceiling of an EAB sensor depends mainly on the electrochemical interrogation strategy. SWV applies staircase potential steps superimposed with square-wave pulses, recording the net difference current to suppress capacitive background [47]. Kinetic differential measurement (KDM) exploits the frequency dependence of the MB electron-transfer rate: because ligand-bound and unbound aptamer conformations have different $k_0$ values, subtracting (or taking the ratio of) currents recorded at a signal-on frequency and a signal-off SWV frequency cancels common-mode drift while amplifying the binding-dependent signal [48,49]. KDM extended operational windows to several hours in blood but cannot decouple sensor-to-sensor manufacturing variation from concentration measurements without individual calibration curves [22].

FFT-EIS was developed to remove this calibration requirement. Roehrich et al. superimposed multi-frequency sinusoidal perturbations on a DC bias and extracted impedance spectra via fast Fourier transform within 1.7 seconds per scan. Equivalent-circuit fitting using a Randles model revealed that the heterogeneous electron transfer rate constant ($k_0$)—which can be extracted by evaluating the charge-transfer resistance (Rct) alongside the double-layer capacitance—responds systematically to ligand concentration, while solution resistance remains essentially invariant [44]. Because $k_0$ is an intrinsic kinetic parameter that is independent of the absolute number of surface-bound methylene blue reporters and relatively insensitive to electrode area variation and electrolyte conductivity fluctuations, it circumvents the two dominant sources of inter-sensor calibration drift—microscopic deviations in electrochemical surface area and variations in self-assembled monolayer packing density—thereby enabling calibration-free readout. In live rats, FFT-EIS interrogation of doxorubicin-targeted EAB sensors achieved inter-animal coefficients of variation below 12% without individual precalibration. Calibration-free readout is a prerequisite for clinical deployment, because recalibration in vivo is impractical [19,50]. Table 2 summarizes key interrogation methods.

**Table 2.** Comparison of electrochemical signal interrogation strategies for in vivo EAB sensors.

| Method | Operating Principle | Key Advantages | Key Limitations | Ref |
|---|---|---|---|---|
| **SWV** | Staircase potential + symmetrical pulse; net forward-minus-reverse current measured | Mature instrumentation; ~10 s resolution; compatible with portable potentiostats | Baseline drift from non-specific adsorption; individual calibration required | [22] |
| **KDM (dual-frequency SWV)** | Signal difference at high and low SWV frequencies; exploits $k_0$ frequency dependence of bound vs unbound aptamer | Suppresses common-mode drift; extends operational window to several hours | Partial calibration still required; frequency optimization is target-specific | [22] |
| **FFT-EIS** | Multi-frequency sinusoidal perturbation superimposed on DC bias; Randles-model Rct extracted via FFT | Calibration-free across sensors; <2 s resolution; decouples concentration from electrode geometry | Complex data pipeline; requires high-bandwidth electronics; hardware | [44] |

 doi:10.20944/preprints202606.0143.v1



| | | | | |
|---|---|---|---|---|
| | | | miniaturization remains a challenge | |
| **Chronoamperometry** | Step potential; measures current decay transient at sub-second timescale | Subsecond data acquisition; very low hardware complexity | Background-current subtraction critical; surface-state sensitive; limited published in vivo anthracycline data | [45] [46] |

SWV, square-wave voltammetry; KDM, kinetic differential measurement; FFT-EIS, fast Fourier transform electrochemical impedance spectroscopy; Rct, charge-transfer resistance.

## 3. In Vivo Multi-Compartment Pharmacokinetics and Feedback Drug Delivery

### *3.1. Simultaneous Plasma and Interstitial-Fluid Pharmacokinetic Monitoring*

Anthracyclines exhibit triphasic plasma pharmacokinetics with a rapid distribution half-life on the order of minutes, reflecting extensive partitioning into tissues, including the tumor interstitium and cardiomyocytes, followed by slower metabolic elimination over tens of hours. The plasma-to-tissue concentration gradient and its time course determine organ-specific exposure and therefore the balance between antitumor efficacy and cardiotoxicity. Conventional monitoring informs only plasma levels [10,19].

Emmons et al. addressed this gap by implanting two EAB sensors simultaneously in anesthetized rats, one in the jugular vein and a second in the subcutaneous interstitial space, each sampling at approximately twelve-second intervals [28]. The resulting data revealed a reproducible plasma-to-ISF lag of 30–60 minutes, with ISF peak concentrations consistently 30–40% lower than plasma Cmax. This temporal and quantitative offset arises from restricted transmembrane diffusion and lymphatic clearance kinetics in the interstitial compartment [51]. Plasma sampling at the one-hour mark, the most common clinical collection point, underestimates ongoing drug delivery to peripheral tissues, including the myocardium, at that instant [52]. An independent study confirmed seconds-resolved EAB monitoring of irinotecan in rat jugular vein with strong agreement against LC-MS/MS, establishing methodological transferability across structurally diverse chemotherapeutics [48].

### *3.2. Closed-Loop Feedback-Controlled Dosing*

The dual-sensor plasma-ISF pharmacokinetic framework provided the basis to test closed-loop feedback drug delivery. Emmons et al. coupled a jugular-vein EAB sensor to a PID (proportional-integral-derivative) controller operating at a seven-second feedback interval, modulating infusion-pump delivery to maintain a target plasma doxorubicin concentration in live rats [25]. Once the plasma setpoint was achieved, subcutaneous ISF concentrations converged within the expected lag period with a root-mean-square deviation of 8–21% [25]. The inter-sensor agreement between two independent EAB sensors implanted in the same compartment ($R^2$ = 0.95–0.99) validated device reproducibility under in vivo conditions [25].

The closed-loop system worked under anesthesia, but several constraints limit near-term translation. PID control assumes a time-invariant plasma-ISF relationship, which is unlikely in patients with fluctuating hemodynamics, edema, or tumor interstitial hypertension. Cardiotoxicity does not scale monotonically with instantaneous plasma concentration; rather, cumulative exposure, peak rate, and individual susceptibility each contributes independently [53,54]. A clinically meaningful closed-loop algorithm will require multiparameter endpoints incorporating cardiac biomarkers (e.g., high-sensitivity troponin I [55]) alongside real-time drug concentration data, rather than using plasma concentration alone as the control variable [56].

### *3.3. Multiplexed Sensing and Tumor Microenvironment Monitoring*

 doi:10.20944/preprints202606.0143.v1



Anthracyclines are rarely administered as single agents; the AC (doxorubicin plus cyclophosphamide) and TAC regimens widely used in breast cancer neoadjuvant chemotherapy require simultaneous concentration monitoring of structurally distinct agents [59–61]. Multiplexed EAB platforms address this by spatially segregating aptamers for different targets across a microelectrode array, with differential redox reporters enabling potential-domain discrimination of simultaneously acquired signals [62–66]. To resolve structurally similar analytes, cross-reactive aptamers have been exploited in two complementary ways. One design pairs a cross-reactive aptamer with a specific aptamer in a dual-channel array, allowing mathematical deconvolution of the overlapped signal [58]. Modulation of electrode surface charge enables quantification based on differential binding responses, without requiring a second aptamer. The latter strategy has been validated directly on the doxorubicin/doxorubicinol pair—two compounds that differ only by a ketone-to-hydroxyl reduction—illustrating its potential for simultaneous monitoring of anthracycline drugs and their cardiotoxic metabolites [11,67].

The tumor microenvironment (TME) adds another layer of difficulty. Solid tumors maintain interstitial pH values of 6.0–6.5 (Warburg acidosis) [68], altering both the protonation state of anthracycline amino sugars (which reduces transmembrane uptake efficiency) and the standard reduction potential of the methylene blue reporter [69]. Studies show that the MB peak potential shifts linearly with pH at approximately −59 mV per unit, close to the Nernstian value for a two-proton, two-electron process [70,71]. Simultaneous recording of MB peak amplitude and peak potential can, in principle, deconvolve drug concentration from local pH, but whether this dual-output strategy retains sufficient discrimination in the complex ionic milieu of tumor ISF remains to be demonstrated under in vivo tumor microenvironment conditions, where competing ionic and redox effects may shift Nernstian MB behavior [72,73]. Table 3 provides a structured comparison of the in vivo EAB performance data for anthracyclines and related chemotherapeutic agents reported in the literature.

**Table 3.** In vivo EAB sensor performance data for anthracycline and related chemotherapeutic monitoring.

| Analyte | Electrode Platform | Dynamic Range | Time Resolution | Compartment | Key Finding | Ref |
|---|---|---|---|---|---|---|
| Doxorubicin | Planar Au, SWV/KDM | 0.1–10 μM | 12 s | Plasma + subcutaneous ISF | 30–60 min lag between plasma and ISF; first in vivo simultaneous plasma–ISF PK resolved | [28] |
| Daunorubicin | Nanoporous Au, SWV | 0.004–450 μM | ~30 s | In vivo rat blood (iv) | PK parameters (t½, Cmax, AUC) resolved in real time; 3–5× signal gain vs planar Au | [23] |
| Doxorubicin | Hydrogel-protected Au/aptamer | 0.1–50 μM | 30 s | Rabbit whole blood (ex vivo) | Hydrogel preserves function in complex matrix; 7-day storage stability; biofouling suppressed | [24] |
| Irinotecan (CPT-11) | Planar Au, SWV | 0.5–15 μM | 20 s | Rat jugular vein | Validated against LC-MS/MS; supports high-resolution temporal tracking | [48] |
| Methotrexate | Au microelectrode, SWV | 0.01–5 μM | 10 s | Rat jugular vein | Seconds-resolved tracking of plasma PK; revealed large inter-subject differences in exposure | [57] |
| Methotrexate & DAMPA | Dual-channel Au array, SWV | Target specific | ~10 s | Whole blood / Complex buffer | Differential metabolite discrimination; cross-reactivity addressed by mathematical deconvolution | [58] |
| Doxorubicin (closed-loop) | Planar Au + PID algorithm | 0.5–4 μM | 7 s feedback | Rat jugular vein + ISF | Plasma setpoint maintained; ISF tracked within 8–21% RMSE; inter-sensor $R^2$ = 0.95–0.99 | [25] |

 doi:10.20944/preprints202606.0143.v1



ISF, interstitial fluid; KDM, kinetic differential measurement; SWV, square-wave voltammetry; RMSE, root-mean-square error; PK, pharmacokinetics; DAMPA, 2,4-diamino-N10-methylpteroic acid; PID, proportional-integral-derivative.

## 4. In Vivo Stability: Mechanisms of Signal Drift and Engineering Countermeasures

### *4.1. Biphasic Signal Decay and Its Mechanistic Basis*

Signal drift limits continuous EAB deployment to less than 24 hours under standard conditions [74]. Leung et al. resolved this into two mechanistically independent phases through systematic manipulation of blood components and interrogation protocols [72]. The initial exponential decay, occurring within approximately ninety minutes of blood contact, was determined to be driven by high-molecular-weight proteins (>100 kDa) through the use of size-fractionated serum, confirming that macromolecular fouling and enzymatic aptamer cleavage act as primary drivers [72,74]. Non-specific adsorption of serum proteins contributes a parallel blocking component that sterically hinders conformational dynamics and reduces MB electron-transfer efficiency [72,74]. The second, linear decay phase persisted even in enzyme-free buffers but was suspended when electrochemical interrogation was paused, identifying reductive SAM desorption driven by the applied potential as its cause [75]. Sustained in vivo operation therefore requires independent engineering solutions: enzymatic resistance for the exponential phase, and optimized scanning protocols (reduced potential window, lower interrogation frequency) for the linear phase.

### *4.2. Xenonucleic Acid Substitution for Enzymatic Resistance*

Phosphorothioate backbone modification and 3′-inversion termini provide partial resistance to exonuclease activity but do not eliminate recognition by the predominant endonucleases in blood [66]. Backbone replacement with xenonucleic acids (XNA), non-natural sugar or backbone chemistries that blood nucleases lack the active-site geometry to cleave, more directly addresses enzymatic degradation. Leung et al. initially replaced the DNA backbone of a tobramycin aptamer with 2′-O-methyl RNA, a chemically modified nucleic acid that blood endonucleases cannot efficiently cleave, classified functionally as a xenonucleic acid in the EAB literature (though truly synthetic XNA backbones such as threose nucleic acid and hexitol nucleic acid have not yet been demonstrated in vivo for any EAB system), confirming that this modification attenuated in vivo EAB signal drift by more than 50% relative to DNA sensors. The 2′-O-methyl variants unexpectedly exhibited higher affinity than the DNA parent, attributable to the C3′-endo sugar pucker more closely matching the RNA conformation sampled during the original SELEX, recovering rigid binding-pocket geometry [77]. Building on this stability, Son et al. subsequently deployed an XNA-modified sensor in a live rat for seven consecutive days, accumulating more than 47,000 measurements at 12.8-s resolution [76].

The XNA strategy carries practical constraints. Not all DNA-to-XNA substitution patterns preserve high-affinity binding; optimal modification patterns are target-specific and require iterative synthesis and characterization. XNA phosphoramidites cost more to synthesize than natural-backbone monomers. No published report yet describes a high-affinity 2′-O-methyl RNA or full-XNA aptamer for doxorubicin or daunorubicin, limiting direct transfer of the XNA stability advantage to the anthracycline monitoring context.

4.3 Antifouling Coatings: Hydrogels and Zwitterionic BrushesPhysical exclusion and thermodynamic repulsion are complementary ways to limit fouling [78]. Table 4 summarizes the principal antifouling strategies, their mechanisms, and associated trade-offs for in vivo EAB sensors. Tetra-polyethylene glycol (tetra-PEG) hydrogels form a sieving network that physically blocks proteins larger than the mesh-size cutoff; Nguyen TT et al. showed that tetra-PEG coated EAB sensors in undiluted whole blood reduced drift from ~25.1% to ~5.7% over eight hours while maintaining comparable signal gain for the target molecule [79]. Combinatorial acrylamide hydrogels selected by

 doi:10.20944/preprints202606.0143.v1



machine learning from a large copolymer library were found to outperform PEG and standard zwitterionic coatings on sensors implanted intravenously in rodents, showing that computational screening can identify effective coating compositions [78]. Hydrogel-protected EAB detection of doxorubicin was demonstrated in undiluted whole blood [24], confirming functional biofouling suppression in the most clinically relevant matrix [80].

Zwitterionic polymer brushes, typically polysulfobetaine methacrylate (SBMA) or polycarboxybetaine, resist protein adsorption through a tightly organized hydration layer [81,82]. Yao et al. showed that microgel-reinforced carboxybetaine/sulfobetaine hydrogels reduced fibrin deposition and hemolysis on blood-contacting surfaces implanted in rats and rabbits [81]. Duan et al. integrated SBMA with polydopamine and a gold nanoparticle/MXene nanocomposite, demonstrating antifouling performance maintained across temperature, pH, and mechanical stress variations [83]. When zwitterionic brush grafting density is too high, polymer chains physically constrain aptamer conformational transitions, reducing absolute signal gain despite effective fouling suppression [82]. Resolving this density-function conflict through sub-nanometer spatial control of aptamer and polymer chain positioning remains a challenge for co-immobilized aptamer–polymer interfaces [21].

**Table 4.** Antifouling strategies for in vivo EAB sensors. Mechanisms, performance, and trade-offs.

| Strategy | Mechanism | Drift Reduction | Effect on Signal Gain | Demonstrated Matrix | Key Limitation | Ref |
|---|---|---|---|---|---|---|
| **Tetra-PEG hydrogel** | Physical sieving; mesh excludes proteins above MW cutoff | ~75% drift reduction over 8 h | Near-unity (~95% preserved) | Undiluted saliva; serum | Mesh must be tuned per analyte MW; slows response kinetics | [79] |
| **Combinatorial acrylamide hydrogel** | ML-guided copolymer selection; combined repulsion | Exceeds PEG and standard zwitterionic controls | Preserved when composition optimized | In vivo iv implantation in rodents | Composition requires ML-assisted design; not yet standardized | [78] |
| **SBMA zwitterionic brush** | Dense hydration layer; thermodynamic exclusion of proteins | Significant albumin/fibrinogen adsorption reduction | Reduced at high grafting density | In vitro and in vivo (hours) | Grafting density vs aptamer conformational freedom trade-off | [83] |
| **Microgel-reinforced CB/SB hydrogel** | Mechanical reinforcement + dual-zwitterion chemistry | Reduced fibrin deposition; low hemolysis | Compatible with electrochemical readout | Ex vivo rat/rabbit blood contact | Complex fabrication; adhesion requires roughened electrode surfaces | [81] |
| **2′-O-methyl RNA (XNA)** | Backbone not recognized by blood nucleases; eliminates enzymatic cleavage | >50% drift reduction (Leung); 7-day continuous operation (Son) | Often improved vs DNA parent (better Kd) | In vivo rat blood (7 days) | Target-specific optimization needed; high synthesis cost; no anthracycline-specific XNA aptamer published | [77] |
| **Collagen + RNase inhibitor membrane** | Physical barrier + enzymatic inhibition | RNA aptamer half-life extended in serum | Maintained over 6 h in serum | In vitro serum | In vivo inhibitor persistence and biocompatibility unconfirmed | [84] |

 doi:10.20944/preprints202606.0143.v1



Notes: SBMA, polysulfobetaine methacrylate; CB/SB, carboxybetaine/sulfobetaine; XNA, xenonucleic acid; PEG, polyethylene glycol; ML, machine learning.

## 5. Toward Clinical Translation: Device Formats and Regulatory Pathways

### *5.1. Intravascular Implants Versus Wearable Microneedle Arrays*

Two device formats have been proposed for clinical monitoring, each with distinct risk profiles [85]. Intravascular EAB sensors access plasma directly—the pharmacokinetically most informative compartment, but expose the sensing surface to high shear stress, platelet-rich flow, and protein deposition [74]. Long-term catheter placement invites thrombosis, bloodstream infection, and progressive foreign-body encapsulation [43,86–88]. Engineering countermeasures include low-thrombogenic antifouling coatings, ultrasound-powered wireless transmission to avoid transcutaneous wires, and miniaturized implantable potentiostats [89].

Transdermal microneedle arrays sample ISF at 200–700 μm depth without vascular access, reducing infection and thrombosis risk [73]. Zhu et al. addressed mechanical resilience using a nanostructured bioelectrode (RNB) microneedle array, gold-deposited nanocavity surfaces that maintained electrochemical performance through hundreds of insertion-retraction cycles with less than 15% signal degradation, enabling six days of continuous preclinical monitoring in a freely moving rat [90]. Beyond mechanical stability, microneedle-based anthracycline TDM faces the fundamental pharmacological challenge that the plasma-ISF concentration ratio is not fixed: local inflammation, edema, and altered tissue perfusion, common in chemotherapy patients, shift it unpredictably [28]. Patient-specific calibration using concurrent venipuncture samples during an initial sensor initialization period would still be required for clinical-grade use [91].

### *5.2. FDA Regulatory Classification and PMA Requirements*

Under FDA device taxonomy, EAB sensors intended for in vivo anthracycline TDM are likely to be classified as Class III, given their direct patient contact in a life-sustaining pharmacotherapy context and their potential to drive algorithmic dosing decisions for a drug class with known lethal cardiotoxicity [92]. Class III designation mandates Premarket Approval (PMA), requiring prospective clinical trial data demonstrating that device use improves patient outcomes, operationalized as reduced cardiotoxicity incidence or improved objective tumor response at equivalent doses. Development timelines often exceed five years from design lock [92].

De Novo classification might apply to sensors used solely for data collection without real-time dosing feedback, but no regulatory precedent exists for intravascular molecular monitoring devices in oncology [92]; Table 5 compares the principal FDA regulatory pathways relevant to EAB-based in vivo TDM devices. Pre-Submission (Q-Sub) engagement with FDA before formal device categorization is advisable, particularly to negotiate acceptable discordance limits versus the LC-MS/MS reference method and to establish the minimum required performance data for the intended clinical claim [93]. Breakthrough Device Designation, available when an unmet clinical need is clearly documentable, could reduce PMA review burden through expedited FDA interaction and review cycles [94].

### *5.3. Emerging Policy Frameworks: In Silico Evidence and Real-Time Clinical Trials*

Two recent FDA policy developments may shorten regulatory timelines. FDA's formal acceptance of in silico modeling data as supporting evidence in device submissions, under FDA Computational Modeling and Simulation (CM&S) guidance and harmonized with the broader New Approach Methodology (NAM) framework, means that computational PK models validated against existing animal data could support the design of human dosing algorithms before large-scale clinical trials [95,96]. For an EAB-driven closed-loop system, this pathway could shorten pre-trial development by replacing some early-phase clinical experiments with validated digital twins of the sensor-controller-patient system [97].

 doi:10.20944/preprints202606.0143.v1



The Real-Time Clinical Trial (RTCT) initiative, launched by FDA in April 2026, allows agency reviewers to access pre-specified safety and efficacy endpoints as data accumulate during an ongoing trial [98]. This approach aims to reduce the administrative "dead time" between trial phases and may shorten regulatory review [99,100]. Continuous sensor streams fit this trial model: the persistent timestamped data stream from an EAB device can be directed to a regulatory-access cloud platform in real time. AstraZeneca and Amgen have initiated RTCT pilots in oncology [99,101]. Whether RTCT can shorten the PMA timeline for a Class III combination device ultimately depends on how FDA defines the primary efficacy endpoint and on the agency's willingness to accept sensor-measured continuous PK parameters (e.g., Cmax and AUC) as a surrogate for hard cardiac outcomes—a possibility that is consistent with FDA's existing framework for surrogate endpoints [102] and the documented PK/PD relationships for anthracyclines [103], but which has not yet been formally addressed in FDA guidance for sensor-based continuous monitoring in oncology.

**Table 5.** FDA regulatory pathway comparison for EAB-based in vivo therapeutic drug monitoring devices.

| Pathway | Applicable Risk Class | Key Evidence Requirements | Typical Timeline | Implication for Anthracycline EAB | Ref |
|---|---|---|---|---|---|
| **510(k) Premarket Notification** | Class I–II (low–moderate risk) | Substantial equivalence to predicate; no RCT required | 3–12 months | Unlikely to apply; no valid predicate for in vivo chemotherapy monitoring | [104] |
| **De Novo Classification** | Novel low–moderate risk, no predicate | Risk-based special controls; clinical data may be required | 12–24 months | Possible for data-collection-only variant; dosing-feedback functionality triggers Class III | [105] |
| **Premarket Approval (PMA)** | Class III (high risk, life-sustaining) | Multicenter RCT; demonstrated clinical benefit (cardiotoxicity reduction or improved response) | 4–8 years total | Most probable pathway; requires robust outcome data | [92] |
| **Breakthrough Device Designation** | Any class with unmet clinical need | Expedited review; interactive FDA development; no reduced evidence requirement | Reduces review time ~30% | Applicable; unmet need for real-time anthracycline TDM is well documented | [94] |
| **Real-Time Clinical Trial (RTCT)** | Any class | Continuous pre-specified data stream to FDA reviewers; adaptive endpoints | Pilot phase launched 2026 | Compatible with continuous EAB data streams; may reduce post-trial review lag | [96] |

RCT, randomized controlled trial; FDA, U.S. Food and Drug Administration; PMA, premarket approval; RTCT, real-time clinical trial; CM&S, computational modeling and simulation.

## 6. Conclusions and Future Directions

Over the past decade, EAB sensors have moved from proof-of-concept experiments toward tools that can track pharmacokinetics in vivo [22,50]. EAB sensors can now resolve anthracycline concentration dynamics at seconds-scale resolution across two tissue compartments simultaneously, drive closed-loop dosing in animal models with sub-minute feedback, and, with XNA backbone substitution, operate continuously in vivo for periods approaching a week [25,78]. Calibration-free FFT-EIS interrogation has removed one of the most practically limiting requirements for clinical deployment, and combinatorial antifouling strategies have extended operational lifetimes that once collapsed within hours [44,78].

 doi:10.20944/preprints202606.0143.v1



Three barriers remain. First, data from healthy rodents may not transfer to oncology patients [19,59]. Every published in vivo EAB validation to date has used non-tumor-bearing, anesthetized or freely moving rodents. Anthracycline pharmacokinetics in patients is shaped by hepatic dysfunction, altered protein binding, tumor-associated vascular permeability, and concurrent polypharmacy, all absent from current preclinical models [3,106]. As shown in Figure 2A, dedicated studies in tumor-bearing animals treated with clinically representative regimens are necessary before the ISF-to-plasma concentration relationship can be assigned with sufficient confidence for clinical application [107].

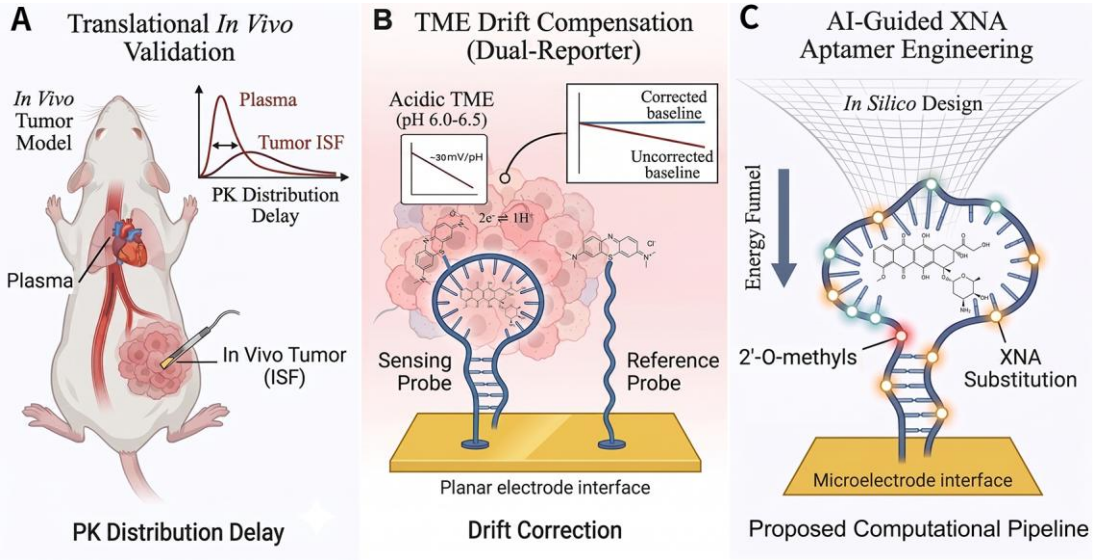


**Figure 2.** Optimization and translational validation of EAB sensors. (A) In vivo validation setup in a mouse model, depicting sensor placement in plasma and tumor ISF to measure pharmacokinetic distribution delays. (B) Proposed dual-reporter drift-compensation strategy. A sensing probe and a reference probe on a planar electrode are intended to compensate for baseline variations in acidic tumor microenvironments (pH 6.0–6.5); in vivo tumor validation remains pending. (C) Computational pipeline for aptamer engineering, indicating target sites for 2′-O-methyl and XNA substitutions.

Second, sensors must be calibrated for acidic, hypoxic tumor tissue. TME acidification (pH 6.0–6.5), elevated interstitial pressure, and hypoxia alter both aptamer binding thermodynamics and redox reporter behavior in ways that EAB sensors calibrated in normal tissue cannot fully account for. As shown in Figure 2B, dual-reporter designs pairing a drug-sensitive channel with a non-binding reference aptamer of identical surface chemistry offer a route to real-time compensation for baseline drift in acidic environments, but such designs have not yet been validated under relevant in vivo tumor microenvironmental conditions [108].

Third, anthracycline-binding aptamers still need targeted engineering. Published XNA and AI-assisted design advances—AptaDiff and RoseTTAFoldNA—have to date been validated against cocaine, tobramycin, vancomycin, or protein targets [34,35]. No high-affinity 2′-O-methyl RNA or full-XNA aptamer for doxorubicin or daunorubicin has yet been reported for in vivo EAB monitoring, despite the need in anthracycline TDM [109]. As shown in Figure 2C, applying the computational design-test-optimize cycle to anthracycline-binding aptamers should be tested next; success would address enzymatic stability, calibration drift, and sensitivity through strategies such as AI-guided XNA substitution [31].

**Author Contributions:** Conceptualization, H.Z. and T.L.; methodology, H.Z., H.W., W.L. and T.L.; investigation, H.Z.; data curation, H.Z.; writing—original draft preparation, H.Z.; writing—review and editing, H.Z., H.W., W.L. and T.L.; visualization, H.Z.; supervision, T.L.; project administration, T.L. All authors have read and agreed to the published version of the manuscript.

 doi:10.20944/preprints202606.0143.v1



**Funding:** This research was funded by the Key Area Project of General Universities in Guangdong Province (No. 2024ZDZX2080).

**Institutional Review Board Statement:** Not applicable.

**Informed Consent Statement:** Not applicable.

**Data Availability Statement:** No new data were created or analyzed in this study. Data sharing is not applicable.

**Acknowledgments:** During the preparation of this manuscript, the authors used Gemini to draw the structures of elements in the illustration based on the authors' own conceptual designs. The authors have reviewed and edited the output and take full responsibility for the content of this publication.

**Conflicts of Interest:** The authors declare no conflicts of interest.

## References

1. Bagdasaryan, A.A.; Chubarev, V.N.; Smolyarchuk, E.A.; Drozdov, V.N.; Krasnyuk, I.I.; Liu, J.; Fan, R.; Tse, E.; Shikh, E.V.; Sukocheva, O.A. Pharmacogenetics of Drug Metabolism: The Role of Gene Polymorphism in the Regulation of Doxorubicin Safety and Efficacy. Cancers 2022, 14, 5436.
2. Minotti, G.; Menna, P.; Salvatorelli, E.; Cairo, G.; Gianni, L. Anthracyclines: molecular advances and pharmacologic developments in antitumor activity and cardiotoxicity. Pharmacol. Rev. 2004, 56, 185–229.
3. Danesi, R.; Fogli, S.; Gennari, A.; Conte, P.; Del Tacca, M. Pharmacokinetic-pharmacodynamic relationships of the anthracycline anticancer drugs. Clin. Pharmacokinet. 2002, 41, 431–444.
4. Saito, K.; Takahata, T.; Nakagawa, J.; Chen, Y.; Saito, K.; Kamata, K.; Tachita, T.; Yamashita, S.; Ueno, K.; Sato, A.; Sakuraba, H.; Niioka, T. Influence of Polymorphisms in Pharmacokinetics-Related Genes on the Areas Under the Plasma Concentration-Time Curves of Doxorubicin and Doxorubicinol in Patients with Diffuse Large B-Cell Lymphoma Receiving CHOP Therapy. Eur. J. Drug Metab. Pharmacokinet. 2025, 50, 219–227.
5. Joerger, M.; Huitema, A.D.; Richel, D.J.; Dittrich, C.; Pavlidis, N.; Briasoulis, E.; Vermorken, J.B.; Strocchi, E.; Martoni, A.; Sorio, R.; Sleeboom, H.P.; Izquierdo, M.A.; Jodrell, D.I.; Fety, R.; de Bruijn, E.; Hempel, G.; Karlsson, M.; Tranchand, B.; Schrijvers, A.H.; Twelves, C.; Beijnen, J.H.; Schellens, J.H.; EORTC-PAMM-NDDG. Population pharmacokinetics and pharmacodynamics of doxorubicin and cyclophosphamide in breast cancer patients: a study by the EORTC-PAMM-NDDG. Clin. Pharmacokinet. 2007, 46, 1051–1068.
6. Lal, S.; Sandanaraj, E.; Wong, Z.W.; Ang, P.C.S.; Wong, N.S.; Lee, E.J.D.; Chowbay, B. CBR1 and CBR3 pharmacogenetics and their influence on doxorubicin disposition in Asian breast cancer patients. Cancer Sci. 2008, 99, 2045–2054.
7. Swain, S.M.; Whaley, F.S.; Ewer, M.S. Congestive heart failure in patients treated with doxorubicin: a retrospective analysis of three trials. Cancer 2003, 97, 2869–2879.
8. Sallustio, B.C.; Boddy, A.V. Is there scope for better individualisation of anthracycline cancer chemotherapy? Br. J. Clin. Pharmacol. 2021, 87, 295–305.
9. Yan, A.; Culp, E.; Perry, J.; Lau, J.T.; MacNeil, L.T.; Surette, M.G.; Wright, G.D. Transformation of the Anticancer Drug Doxorubicin in the Human Gut Microbiome. ACS Infect. Dis. 2018, 4, 68–76.
10. Pashaei, Y.; Mehrabi, M.; Shekarchi, M. A review on various analytical methods for determination of anthracyclines and their metabolites as anti–cancer chemotherapy drugs in different matrices over the last four decades. TrAC Trends Anal. Chem. 2020, 130, 115991.
11. Chairunnisa, D.F.; Harahap, Y.; Juanita, M.; Syafhan, N.F.; Purwanto, D.J. Doxorubicin, doxorubicinol, cardiotoxicity, breast cancer, volumetric absorptive microsampling, LC-MS/MS. Pak. J. Biol. Sci. 2024, 27, 125–131.
12. Emmons, N.A. Advancing personalized medicine with electrochemical aptamer-based (EAB) sensors. Ph.D. Thesis, University of California, Santa Barbara, CA, USA, 2024.
13. Qiu, Y.; Jiang, P.; Huang, Y. Anthracycline-induced cardiotoxicity: mechanisms, monitoring, and prevention. Front. Cardiovasc. Med. 2023, 10, 1242596.

 doi:10.20944/preprints202606.0143.v1




14. Groth, L.; Jorgensen, A.; Serup, J. Cutaneous microdialysis in the rat: insertion trauma and effect of anaesthesia studied by laser Doppler perfusion imaging and histamine release. Skin Pharmacol. Appl. Skin Physiol. 1998, 11, 125–132.
15. Jørgensen, A.R.; Hansen, J.; Bue, M.; Hanberg, P.; Stilling, M. Microdialysis as a sampling tool for the chemotherapeutic agent Doxorubicin. J. Pharm. Biomed. Anal. 2024, 239, 115872.
16. Whitaker, G.; Lunte, C.E. Investigation of microdialysis sampling calibration approaches for lipophilic analytes: doxorubicin. J. Pharm. Biomed. Anal. 2010, 53, 490–496.
17. Kruachottikul, P.; Tea-makorn, P.; Dumrongvute, P.; Hemrungrojn, S.; Nupairoj, N.; Junchaya, O.; Vinayavekhin, S. MediGate: a MedTech product innovation development process from university research to successful commercialization within emerging markets. J. Innov. Entrep. 2024, 13, 71.
18. White, R.J.; Rowe, A.A.; Plaxco, K.W. Re-engineering aptamers to support reagentless, self-reporting electrochemical sensors. Analyst 2010, 135, 589–594.
19. Dauphin-Ducharme, P.; Yang, K.; Arroyo-Currás, N.; Ploense, K.L.; Zhang, Y.; Gerson, J.; Kurnik, M.; Kippin, T.E.; Stojanovic, M.N.; Plaxco, K.W. Electrochemical aptamer-based sensors for improved therapeutic drug monitoring and high-precision, feedback-controlled drug delivery. ACS Sens. 2019, 4, 2832–2837.
20. Fetter, L.C.; McDonough, M.H.; Kippin, T.E.; Plaxco, K.W. Effects of Physiological-Scale Variation in Cations, pH, and Temperature on the Calibration of Electrochemical Aptamer-Based Sensors. ACS Sens. 2024, 9, 6675–6684.
21. Wu, Y.; Plaxco, K.W. On the Design, Fabrication, and Operation of Electrochemical Aptamer-Based Sensors. ACS Sens. 2025, 10, 7218–7230.
22. Arroyo-Currás, N.; Somerson, J.; Vieira, P.A.; Ploense, K.L.; Kippin, T.E.; Plaxco, K.W. Real-time measurement of small molecules directly in awake, ambulatory animals. Proc. Natl. Acad. Sci. U. S. A. 2017, 114, 645–650.
23. Qin, S.N.; Jie, Z.Q.; Chen, L.Y.; Zheng, J.X.; Xie, Y.; Feng, L.; Chen, Z.M.; Salminen, K.; Sun, J.J. Real-time monitoring of daunorubicin pharmacokinetics with nanoporous electrochemical aptamer-based sensors in vivo. Sens. Actuators B Chem. 2024, 411, 135710.
24. Luo, S.; Wu, Q.; Wang, L.; Qu, H.; Zheng, L. Direct detection of doxorubicin in whole blood using a hydrogel-protected electrochemical aptamer-based biosensor. Talanta 2025, 285, 127289.
25. Emmons, N.A.; Duman, Z.; Erdal, M.K.; Hespanha, J.; Kippin, T.E.; Plaxco, K.W. Feedback control over plasma drug concentrations achieves rapid and accurate control over solid-tissue drug concentrations. ACS Pharmacol. Transl. Sci. 2025, 8, 1416–1423.
26. Yang, L.F.; Ling, M.; Kacherovsky, N.; Pun, S.H. Aptamers 101: aptamer discovery and in vitro applications in biosensors and separations. Chem. Sci. 2023, 14, 4961–4978.
27. Tang, T.; Liu, Y.; Jiang, Y. Recent Progress on Highly Selective and Sensitive Electrochemical Aptamer-based Sensors. Chem. Res. Chin. Univ. 2022, 38, 866–878.
28. Emmons, N.A.; Gibson, J.M.; McDonough, M.H.; Gerson, J.; Erdal, M.K.; Leung, K.; Fetter, L.C.; Plaxco, K.W.; Kippin, T.E. Simultaneous, Seconds-Resolved Doxorubicin Measurements in the Blood and Subcutaneous Interstitial Fluid Identify Quantitative Pharmacokinetic Relationships between the Two. ACS Pharmacol. Transl. Sci. 2025, 8, 1347–1358.
29. Schoukroun-Barnes, L.R.; White, R.J. Rationally designing aptamer sequences with reduced affinity for controlled sensor performance. Sensors 2015, 15, 7754–7767.
30. Shaver, A.; Mahlum, J.D.; Scida, K.; Johnston, M.L.; Aller Pellitero, M.; Wu, Y.; Carr, G.V.; Arroyo-Curras, N. Optimization of Vancomycin Aptamer Sequence Length Increases the Sensitivity of Electrochemical, Aptamer-Based Sensors In Vivo. ACS Sens. 2022, 7, 3895–3905.
31. Nguyen, M.D.; Osborne, M.T.; Prevot, G.T.; Churcher, Z.R.; Johnson, P.E.; Simine, L.; Dauphin-Ducharme, P. Truncations and in silico docking to enhance the analytical response of aptamer-based biosensors. Biosens. Bioelectron. 2024, 246, 116680.
32. White, R.J.; Phares, N.; Lubin, A.A.; Xiao, Y.; Plaxco, K.W. Optimization of electrochemical aptamer-based sensors via optimization of probe packing density and surface chemistry. Langmuir 2008, 24, 10513–10518.

 doi:10.20944/preprints202606.0143.v1




33. Li, Z.; Lv, Y.; Duan, X.; Liu, B.; Zhao, Y. Highly Uniform DNA Monolayers Generated by Freezing-Directed Assembly on Gold Surfaces Enable Robust Electrochemical Sensing in Whole Blood. Angew. Chem. Int. Ed. 2023, 62, e202312975.
34. Wang, Z.; Liu, Z.; Zhang, W.; Li, Y.; Feng, Y.; Lv, S.; Diao, H.; Luo, Z.; Yan, P.; He, M.; Li, X. AptaDiff: de novo design and optimization of aptamers based on diffusion models. Brief. Bioinform. 2024, 25, bbae517.
35. Baek, M.; McHugh, R.; Anishchenko, I.; Jiang, H.; Baker, D.; DiMaio, F. Accurate prediction of protein–nucleic acid complexes using RoseTTAFoldNA. Nat. Methods 2024, 21, 117–121.
36. iGEM Team Heidelberg 2015. MAWS. Available online: https://2015.igem.org/Team:Heidelberg/software/maws (accessed on 28 May 2026).
37. iGEM Team DTU-Denmark 2023. AptaLoop. Available online: https://2023.igem.wiki/dtu-denmark/software (accessed on 28 May 2026).
38. Fu, K.; Seo, J.W.; Kesler, V.; Maganzini, N.; Wilson, B.D.; Eisenstein, M.; Murmann, B.; Soh, H.T. Accelerated Electron Transfer in Nanostructured Electrodes Improves the Sensitivity of Electrochemical Biosensors. Adv. Sci. 2021, 8, e2102495.
39. Jahani, P.M.; Nejad, F.G.; Zaimbashi, R.; Tajik, S.; Beitollahi, H. Enhanced voltammetric determination of daunorubicin by modifying the surface of screen-printed carbon electrode. Nanochem. Res. 2025, 10, 416–427.
40. Huldin, G.F.; Huang, J.M.; Fu, K.Y.X. Nanoconfined constructs for electrochemical aptamer-based biosensing. Curr. Opin. Electrochem. 2025, 51, 101695.
41. Choudhury, S.; Zafar, S.; Deepak, D.; Panghal, A.; Lochab, B.; Roy, S.S. A surface modified laser-induced graphene based flexible biosensor for multiplexed sweat analysis. J. Mater. Chem. B 2025, 13, 274–287.
42. De Chiara, B.; Del Duca, F.; Hussain, M.Z.; Kratky, T.; Banerjee, P.; Dummert, S.V.; Khoshouei, A.; Chanut, N.; Peng, H.; Al Boustani, G.; Hiendlmeier, L.; Jinschek, J.; Ameloot, R.; Dietz, H.; Wolfrum, B. Laser-Induced Metal-Organic Framework-Derived Flexible Electrodes for Electrochemical Sensing. ACS Appl. Mater. Interfaces 2025, 17, 3772–3784.
43. Veiseh, O.; Vegas, A.J. Domesticating the foreign body response: Recent advances and applications. Adv. Drug Deliv. Rev. 2019, 148, 148–161.
44. Roehrich, B.; Leung, K.K.; Gerson, J.; Kippin, T.E.; Plaxco, K.W.; Sepunaru, L. Calibration-Free, Seconds-Resolved In Vivo Molecular Measurements using Fourier-Transform Impedance Spectroscopy Interrogation of Electrochemical Aptamer Sensors. ACS Sens. 2023, 8, 3051–3059.
45. Arroyo-Currás, N.; Dauphin-Ducharme, P.; Ortega, G.; Ploense, K.L.; Kippin, T.E.; Plaxco, K.W. Subsecond-resolved molecular measurements in the living body using chronoamperometrically interrogated aptamer-based sensors. ACS Sens. 2018, 3, 360–366.
46. Riordan, K.T.; Yang, K.; Brazelton, E.; Eslami, M.A.; Copenhaver, A.; Esmaeili, F.; Flynn, C.D.; Wu, Z.; Isaacson, S.E.; Chang, D.; Cabezas, M.D.; Juska, V.; Das, J.; Sargent, E.H.; Kelley, S.O. Dual-Chronoamperometry Drift Correction for Electrochemical Sensors. ACS Sens. 2025, 10, 7051–7059.
47. Verrinder, E.; Leung, K.K.; Erdal, M.K.; Sepunaru, L.; Plaxco, K.W. Comparison of voltammetric methods used in the interrogation of electrochemical aptamer-based sensors. Sens. Diagn. 2024, 3, 95–103.
48. Idili, A.; Arroyo-Curras, N.; Ploense, K.L.; Csordas, A.T.; Kuwahara, M.; Kippin, T.E.; Plaxco, K.W. Seconds-resolved pharmacokinetic measurements of the chemotherapeutic irinotecan in situ in the living body. Chem. Sci. 2019, 10, 8164–8170.
49. Ferguson, B.S.; Hoggarth, D.A.; Maliniak, D.; Ploense, K.; White, R.J.; Woodward, N.; Hsieh, K.; Bonham, A.J.; Eisenstein, M.; Kippin, T.E.; Plaxco, K.W.; Soh, H.T. Real-time, aptamer-based tracking of circulating therapeutic agents in living animals. Sci. Transl. Med. 2013, 5, 213ra165.
50. Downs, A.M.; Plaxco, K.W. Real-Time, In Vivo Molecular Monitoring Using Electrochemical Aptamer Based Sensors: Opportunities and Challenges. ACS Sens. 2022, 7, 2823–2832.
51. Wiig, H.; Swartz, M.A. Interstitial fluid and lymph formation and transport: physiological regulation and roles in inflammation and cancer. Physiol. Rev. 2012, 92, 1005–1060.
52. Huang, W.; Xu, R.; Zhou, B.; Lin, C.; Guo, Y.; Xu, H.; Guo, X. Clinical Manifestations, Monitoring, and Prognosis: A Review of Cardiotoxicity After Antitumor Strategy. Front. Cardiovasc. Med. 2022, 9, 912329.

 doi:10.20944/preprints202606.0143.v1




53. Finolezzi, E.; Torromeo, C.; Vincenzi, B.; Avvisati, G. Anthracycline cardiotoxicity. Clin. Ter. 2003, 154, 115–121.
54. Cejas, R.B.; Petrykey, K.; Sapkota, Y.; Burridge, P.W. Anthracycline Toxicity: Light at the End of the Tunnel? Annu. Rev. Pharmacol. Toxicol. 2024, 64, 115–134.
55. Henriksen, P.A.; Hall, P.; MacPherson, I.R.; Joshi, S.S.; Singh, T.; Maclean, M.; Lewis, S.; Rodriguez, A.; Fletcher, A.; Everett, R.J.; Stavert, H.; Broom, A.; Eddie, L.; Primrose, L.; McVicars, H.; McKay, P.; Borley, A.; Rowntree, C.; Lord, S.; Collins, G.; Radford, J.; Guppy, A.; Williams, M.C.; Japp, A.; Payne, J.R.; Newby, D.E.; Mills, N.L.; Oikonomidou, O.; Lang, N.N. Multicenter, Prospective, Randomized Controlled Trial of High-Sensitivity Cardiac Troponin I-Guided Combination Angiotensin Receptor Blockade and Beta-Blocker Therapy to Prevent Anthracycline Cardiotoxicity: The Cardiac CARE Trial. Circulation 2023, 147, 1680–1690.
56. Alkofide, H.; Alnaim, L.; Alorf, N.; Alessa, W.; Bawazeer, G. Cardiotoxicity and cardiac monitoring among anthracycline-treated cancer patients: a retrospective cohort study. Cancer Manag. Res. 2021, 13, 5149–5159.
57. Chamorro-Garcia, A.; Gerson, J.; Flatebo, C.; Fetter, L.; Downs, A.M.; Emmons, N.; Ennis, H.L.; Milosavić, N.; Yang, K.; Stojanovic, M.; Ricci, F.; Kippin, T.E.; Plaxco, K.W. Real-Time, Seconds-Resolved Measurements of Plasma Methotrexate In Situ in the Living Body. ACS Sens. 2023, 8, 150–157.
58. Nguyen, M.-D.; Yang, K.-A.; Coote, L.N.; Vu, C.; Shoara, A.; Johnson, P.E.; Stojanovic, M.N.; Dauphin-Ducharme, P. Exploiting cross-reactivity for selective chemotherapy monitoring: A differential electrochemical aptamer approach. ChemRxiv 2026, preprint.
59. Cardoso, F.; Kyriakides, S.; Ohno, S.; Penault-Llorca, F.; Poortmans, P.; Rubio, I.T.; Zackrisson, S.; Senkus, E. Early breast cancer: ESMO Clinical Practice Guidelines for diagnosis, treatment and follow-up. Ann. Oncol. 2019, 30, 1194–1220.
60. Waks, A.G.; Winer, E.P. Breast Cancer Treatment: A Review. JAMA 2019, 321, 288–300.
61. Fisher, B.; Brown, A.; Mamounas, E.; Wieand, S.; Robidoux, A.; Margolese, R.G.; Cruz, A.B., Jr.; Fisher, E.R.; Wickerham, D.L.; Wolmark, N.; DeCillis, A.; Hoehn, J.L.; Lees, A.W.; Dimitrov, N.V. Effect of preoperative chemotherapy on local-regional disease in women with operable breast cancer: findings from National Surgical Adjuvant Breast and Bowel Project B-18. J. Clin. Oncol. 1997, 15, 2483–2493.
62. Sen, D.; Volya, N.; Muhammed, Y.; Lazenby, R.A. Fabrication and Characterization of a Tunable Microelectrode Array Probe for Simultaneous Multiplexed Electrochemical Detection. Anal. Chem. 2025, 97, 7702–7710.
63. Liu, Y.; Liu, Y.; Matharu, Z.; Rahimian, A.; Revzin, A. Detecting multiple cell-secreted cytokines from the same aptamer-functionalized electrode. Biosens. Bioelectron. 2015, 64, 43–50.
64. Grabowska, I.; Hepel, M.; Kurzatkowska-Adaszynska, K. Advances in Design Strategies of Multiplex Electrochemical Aptasensors. Sensors 2021, 21, 161.
65. Chang, Y.C.; Arnould, B.; Heemstra, J.M.; Moeller, K.D. Developing Microelectrode Arrays for the Point-of-Care Multiplex Detection of Metabolites. Anal. Chem. 2024, 96, 14571–14580.
66. Liu, Y.; Ma, Q.; Zhu, F.; Jin, Y.; Ni, J.; Jiang, Y. Chemically engineered phosphorothioated aptamer for ultrastable dopamine sensing in biomimetic brain. CCS Chem. 2025, 7, 2276–2283.
67. Kesler, V.; Fu, K.; Chen, Y.; Park, C.H.; Eisenstein, M.; Murmann, B.; Soh, H.T. Tailoring electrode surface charge to achieve discrimination and quantification of chemically similar small molecules with electrochemical aptamers. Adv. Funct. Mater. 2023, 33, 2370001.
68. de la Cruz-Lopez, K.G.; Castro-Munoz, L.J.; Reyes-Hernandez, D.O.; Garcia-Carranca, A.; Manzo-Merino, J. Lactate in the Regulation of Tumor Microenvironment and Therapeutic Approaches. Front. Oncol. 2019, 9, 1143.
69. Trebinska-Stryjewska, A.; Swiech, O.; Opuchlik, L.J.; Grzybowska, E.A.; Bilewicz, R. Impact of Medium pH on DOX Toxicity toward HeLa and A498 Cell Lines. ACS Omega 2020, 5, 7979–7986.
70. Sabbagh, B.; Khan, M.I.; Kim, G.; Nandhakumar, P.; Chiu, L.; Zheng, H.; Jakasania, A.; Perez, V.; Saha, T.; Park, M.; Wang, J. Self-Correction of pH-Induced Signal Variations in Methylene Blue-Labeled Aptamer Electrochemical Biosensors: Wearable Cortisol Detection in Sweat. ACS Sens. 2026, 11, 3505–3515.

 doi:10.20944/preprints202606.0143.v1




71. Yang, Y.; Gao, X.; Widdicombe, B.; Zhang, X.; Zielinski, J.L.; Cheng, T.; Gunatilaka, A.; Leung, K.K.; Plaxco, K.W.; Rajasekharan Unnithan, R.; Stewart, A.G. Dual-Purpose Aptamer-Based Sensors for Real-Time, Multiplexable Monitoring of Metabolites in Cell Culture Media. ACS Nano 2024, 18, 26127–26139.
72. Leung, K.K.; Downs, A.M.; Ortega, G.; Kurnik, M.; Plaxco, K.W. Elucidating the Mechanisms Underlying the Signal Drift of Electrochemical Aptamer-Based Sensors in Whole Blood. ACS Sens. 2021, 6, 3340–3347.
73. Bakhshandeh, F.; Zheng, H.; Barra, N.G.; Sadeghzadeh, S.; Ausri, I.; Sen, P.; Keyvani, F.; Rahman, F.; Quadrilatero, J.; Liu, J.; Schertzer, J.D.; Soleymani, L.; Poudineh, M. Wearable Aptalyzer Integrates Microneedle and Electrochemical Sensing for In Vivo Monitoring of Glucose and Lactate in Live Animals. Adv. Mater. 2024, 36, e2313743.
74. Pham, J.D.; Fetter, L.C.; Gerson, J.; Kippin, T.E.; Plaxco, K.W.; Leung, K.K. On the Blood Components Contributing to the Drift of Electrochemical Aptamer-Based Biosensors. ACS Sens. 2025, 10, 5160–5165.
75. Watkins, Z.; Karajic, A.; Young, T.; White, R.; Heikenfeld, J. Week-Long Operation of Electrochemical Aptamer Sensors: New Insights into Self-Assembled Monolayer Degradation Mechanisms and Solutions for Stability in Serum at Body Temperature. ACS Sens. 2023, 8, 1119–1131.
76. Son, K.; Gibson, J.M.; Gerson, J.; Leung, K.K.; Stocco, M.; Lu, Y.; Kippin, T.E.; Plaxco, K.W. Continuous, Week-Long, Seconds-Resolved In Vivo Drug Measurements Performed with a Xenonucleic Acid-Employing Electrochemical, Aptamer-Based Sensor. J. Am. Chem. Soc. 2026, 148, 10016–10025.
77. Leung, K.K.; Gerson, J.; Emmons, N.; Heemstra, J.M.; Kippin, T.E.; Plaxco, K.W. The Use of Xenonucleic Acids Significantly Reduces the In Vivo Drift of Electrochemical Aptamer-Based Sensors. Angew. Chem. Int. Ed. 2024, 63, e202316678.
78. Chan, D.; Chien, J.C.; Axpe, E.; Blankemeier, L.; Baker, S.W.; Swaminathan, S.; Piunova, V.A.; Zubarev, D.Y.; Maikawa, C.L.; Grosskopf, A.K.; Mann, J.L.; Soh, H.T.; Appel, E.A. Combinatorial Polyacrylamide Hydrogels for Preventing Biofouling on Implantable Biosensors. Adv. Mater. 2022, 34, e2109764.
79. Nguyen, T.T.; Mendes, A.X.; Pithaih, V.; Bellette, H.F.F.; Coimbra Pimenta, T.; Moulton, S.E.; Rath, R.J.; Greene, G.W.; Plaxco, K.W.; Silva, S.M. Tetra-Polyethylene Glycol Hydrogel Coating Enhances the Performance and Stability of Electrochemical Sensors in Complex Biological Matrices. ACS Appl. Mater. Interfaces 2026, 18, 25481–25490.
80. Li, S.; Dai, J.; Zhu, M.; Arroyo-Currás, N.; Li, H.; Wang, Y.; Wang, Q.; Lou, X.; Kippin, T.E.; Wang, S.; Plaxco, K.W.; Li, H.; Xia, F. Implantable Hydrogel-Protective DNA Aptamer-Based Sensor Supports Accurate, Continuous Electrochemical Analysis of Drugs at Multiple Sites in Living Rats. ACS Nano 2023, 17, 18525–18538.
81. Yao, M.; Wei, Z.; Li, J.; Guo, Z.; Yan, Z.; Sun, X.; Yu, Q.; Wu, X.; Yu, C.; Yao, F.; Feng, S.; Zhang, H.; Li, J. Microgel reinforced zwitterionic hydrogel coating for blood-contacting biomedical devices. Nat. Commun. 2022, 13, 5339.
82. Trowbridge, A.J.; Huldin, G.F.; Pyo, M.; Jordan, K.M.; Rincon, M.A.; Kim, T.; Webber, M.J.; Gao, H.F.; Park, C.H.; Fu, K.X. Zwitterionic Polymer Brushes Inside Nanoporous Gold Electrodes Enable Fouling-Resistant Electrochemical Biosensing. ACS Appl. Polym. Mater. 2025, 7, 15241–15254.
83. Duan, H.; Peng, S.; He, S.; Tang, S.-Y.; Goda, K.; Wang, C.H.; Li, M. Antifouling zwitterionic coating enhances electrochemical aptamer-based sensors for therapeutic drug monitoring. Nano Today 2026, 60, 102892.
84. Santos-Cancel, M.; White, R.J. Collagen Membranes with Ribonuclease Inhibitors for Long-Term Stability of Electrochemical Aptamer-Based Sensors Employing RNA. Anal. Chem. 2017, 89, 5598–5604.
85. Arroyo-Currás, N.; Dauphin-Ducharme, P.; Scida, K.; Chávez, J.L. From the beaker to the body: translational challenges for electrochemical, aptamer-based sensors. Anal. Methods 2020, 12, 1288–1310.
86. Leung, K.K.; Gerson, J.; Emmons, N.; Roehrich, B.; Verrinder, E.; Fetter, L.C.; Kippin, T.E.; Plaxco, K.W. A tight squeeze: geometric effects on the performance of three-electrode electrochemical-aptamer based sensors in constrained, in vivo placements. Analyst 2023, 148, 1562–1569.
87. Kalashnikov, N.; Barralet, J.; Vorstenbosch, J. Implantable Medical Devices, Biomaterials, and the Foreign Body Response: A Surgical Perspective. J. Biomed. Mater. Res. A 2025, 113, e37983.
88. Luu, C.H.; Nguyen, N.T.; Ta, H.T. Unravelling Surface Modification Strategies for Preventing Medical Device-Induced Thrombosis. Adv. Healthc. Mater. 2024, 13, e2301039.

 doi:10.20944/preprints202606.0143.v1




89. Wang, M.L.; Yeon, P.; Mofidfar, M.; Chamberlayne, C.; Xu, H.; Annes, J.P.; Zare, R.N.; Arbabian, A. A Wireless Implantable Closed-Loop Electrochemical Drug Delivery System. IEEE Trans. Biomed. Circuits Syst. 2025, 19, 777–790.
90. Zhu, J.; Cheng, X.; Bahramian, M.; Yao, K.; Li, Z.; Hu, B.; Wu, T.Y.; Sabet, K.A.; Cui, J.; Tan, J.; Fang, J.; Li, Y.; Ho, C.; Ng, J.; Sung, A.; Romero, I.; Lin, S.; Zhao, Y.; Zhang, K.; Chaiyakul, R.; Yousefi, H.; Flynn, C.D.; Das, J.; Jelinek, D.; Voisin, L.; Ambrus, A.; Zhang, A.; Chi, Y.; Chen, Y.; Liu, C.; Coller, H.A.; Wu, B.M.; Suthana, N.; Kelley, S.O.; Milla, C.; Kurtz, I.; Emaminejad, S. Resilient nanostructured bioanalytic microneedle longitudinally monitors preclinical renal and hepatic drug clearance and dysfunction. Sci. Transl. Med. 2026, 18, eadr5493.
91. Friedel, M.; Werbovetz, B.; Drexelius, A.; Watkins, Z.; Bali, A.; Plaxco, K.W.; Heikenfeld, J. Continuous molecular monitoring of human dermal interstitial fluid with microneedle-enabled electrochemical aptamer sensors. Lab Chip 2023, 23, 3289–3299.
92. FDA. Premarket Approval (PMA). Available online: https://www.fda.gov/medical-devices/premarket-submissions-selecting-and-preparing-correct-submission/premarket-approval-pma (accessed on 28 May 2026).
93. FDA. Requests for Feedback and Meetings for Medical Device Submissions: The Q-Submission Program. Available online: https://www.fda.gov/regulatory-information/search-fda-guidance-documents/requests-feedback-and-meetings-medical-device-submissions-q-submission-program (accessed on 28 May 2026).
94. FDA. Breakthrough Devices Program. Available online: https://www.fda.gov/regulatory-information/search-fda-guidance-documents/breakthrough-devices-program (accessed on 28 May 2026).
95. FDA. Assessing the Credibility of Computational Modeling and Simulation in Medical Device Submissions. Available online: https://www.fda.gov/regulatory-information/search-fda-guidance-documents/assessing-credibility-computational-modeling-and-simulation-medical-device-submissions (accessed on 28 May 2026).
96. FDA. General Considerations for the Use of New Approach Methodologies in Drug Development. Available online: https://www.fda.gov/regulatory-information/search-fda-guidance-documents/general-considerations-use-new-approach-methodologies-drug-development (accessed on 28 May 2026).
97. Corral-Acero, J.; Margara, F.; Marciniak, M.; Rodero, C.; Loncaric, F.; Feng, Y.; Gilbert, A.; Fernandes, J.F.; Bukhari, H.A.; Wajdan, A. The 'Digital Twin'to enable the vision of precision cardiology. Eur. Heart J. 2020, 41, 4556–4564.
98. FDA. FDA Announces Major Steps to Implement Real-Time Clinical Trials. Available online: https://www.fda.gov/news-events/press-announcements/fda-announces-major-steps-implement-real-time-clinical-trials (accessed on 28 May 2026).
99. Makary, M. FDA commissioner: 'Smarter,' real-time clinical trials could transform drug development. Available online: https://www.statnews.com/2026/04/28/fda-clinical-trial-endpoints-real-time-drug-development/ (accessed on 28 May 2026).
100. Logan, M. US pushes real time clinical trials to eliminate "dead time" in approvals. Available online: https://www.bmj.com/content/393/bmj.s855.full (accessed on 28 May 2026).
101. MedPage Today. FDA Says First 'Real-Time' Clinical Trial Is Underway. Available online: https://www.medpagetoday.com/special-reports/exclusives/116634 (accessed on 28 May 2026).
102. FDA. Table of Surrogate Endpoints That Were the Basis of Drug Approval or Licensure. Available online: https://www.fda.gov/drugs/development-resources/table-surrogate-endpoints-were-basis-drug-approval-or-licensure (accessed on 28 May 2026).
103. Ishisaka, T.; Kishi, S.; Okura, K.; Horikoshi, M.; Yamashita, T.; Mitsuke, Y.; Shimizu, H.; Ueda, T. A precise pharmacodynamic study showing the advantage of a marked reduction in cardiotoxicity in continuous infusion of doxorubicin. Leuk. Lymphoma 2006, 47, 1599–1607.
104. FDA. Premarket Notification 510(k). Available online: https://www.fda.gov/medical-devices/premarket-submissions-selecting-and-preparing-correct-submission/premarket-notification-510k (accessed on 28 May 2026).

 doi:10.20944/preprints202606.0143.v1



105. FDA. De Novo Classification Process (Evaluation of Automatic Class III Designation). Available online: https://www.fda.gov/regulatory-information/search-fda-guidance-documents/de-novo-classification-process-evaluation-automatic-class-iii-designation (accessed on 28 May 2026).
106. Magdy, T.; Burridge, P.W. Prime time for doxorubicin-induced cardiotoxicity genetic testing. Pharmacogenomics 2022, 23, 335–338.
107. Müller, M. Monitoring tissue drug levels by clinical microdialysis. Altern. Lab. Anim. 2009, 37, 57–59.
108. Li, H.; Arroyo-Currás, N.; Kang, D.; Ricci, F.; Plaxco, K.W. Dual-Reporter Drift Correction To Enhance the Performance of Electrochemical Aptamer-Based Sensors in Whole Blood. J. Am. Chem. Soc. 2016, 138, 15809–15812.
109. Ou, D.; Yan, H.; Chen, Z. An impedance labeling free electrochemical aptamer sensor based on tetrahedral DNA nanostructures for doxorubicin determination. Mikrochim. Acta 2024, 191, 94.